Encoding complex fields by using a phase-only optical element

Omel Mendoza-Yero,* Gladys Mínguez-Vega, and Jesús Lancis

¹Institut de Noves Tecnologies de la Imatge (INIT), Universitat Jaume I, 12080 Castelló, Spain
*Corresponding author: omendoza@fca.uji.es

We show that the amplitude and phase information from a two-dimensional complex field can be synthesized from a phase-only optical element with micrometric resolution. The principle of the method is based on the combination of two spatially sampled phase elements by using a low-pass filter at the Fourier plane of a $4-f$ optical system. The proposed encoding technique was theoretically demonstrated, as well as experimentally validated with the help of a phase-only spatial light modulator for phase encoding, a conventional CMOS camera to measure the amplitude of the complex field, and a Shack–Hartmann wavefront sensor to determine its phase. © 2014 Optical Society of America

OCIS codes: (120.5060) Phase modulation; (100.5090) Phase-only filters; (260.1960) Diffraction theory.
http://dx.doi.org/10.1364/OL.39.001740

The two-dimensional amplitude $A(x, y)$ and phase $\varphi(x, y)$ of a complex field $U(x, y)$ expressed as $U(x, y) = A(x, y)e^{i\varphi(x,y)}$ can be conveniently rewritten in the form $U(x, y) = Be^{i\theta(x,y)} + Be^{i\vartheta(x,y)}$. In the above expression the terms $\theta(x, y) = \varphi(x, y) + \cos^{-1}[A(x, y)/A_{\max}]$ and $\vartheta(x, y) = \varphi(x, y) - \cos^{-1}[A(x, y)/A_{\max}]$ hold for spatially distributed phase functions, but $B = A_{\max}/2$ is now a constant. Here, $A_{\max}$ is the maximum value of $A(x, y)$. Consequently, the complex field $U(x, y)$ is mainly determined by the phase functions $\theta(x, y)$ and $\vartheta(x, y)$, because the constant term B has influence over only the intensity of the field. From the above analysis, it is apparent that $U(x, y)$ can be retrieved from the coherent superposition of two uniform waves having constant amplitude. This is commonly done with an optical setup able to generate the interference between the two phase elements $\theta(x, y)$ and $\vartheta(x, y)$. However, in practice the above procedure is limited by two fundamental reasons. The first reason is related to the alignment of the interferometer with subpixel accuracy, whereas the second one is its inherent usefulness to synthesize the complex field $U(x, y)$ with a single phase element. In particular, the former handicap has been widely investigated, developing methods for encoding amplitude and phase into phase-only filters [1–9]. Applications of phase-only filters include, but are not limited to, pattern recognition [10,11], correlation discrimination [12], optical encryption [13], shaping of femtosecond pulses [14], or research on non-diffracting speckle fields [15].

Early in 1978, Hsueh and Sawchuk used the phase functions $\theta(x, y)$ and $\vartheta(x, y)$ (for $A_{\max} \equiv 1$, and then $B = 1/2$) to generate double-phase holograms (DPHs) implemented into binary devices [16]. Basically, in DPHs the phase functions $\theta(x, y)$ and $\vartheta(x, y)$, encoded into a single hologram, are suited combined to produce the desired complex field $U(x, y)$. Recent advances in this topic show that phase coding techniques based on the principle of DPH can provide a reasonable good approximation to encode complex fields into a single static optical element or a dynamical optical device, e.g., a phase-only spatial light modulator (SLM). Regarding this point, in 2003 a modification of DPH technique allowed Arrizón

to encode an arbitrary complex function with a twisted nematic liquid-crystal display [17]. Based on the DPH configuration, Arrizón also theoretically introduced in the same year a single-pixel on-axis technique to encode complex fields [18]. Here, it should be noted that the phase modulation proposed in [18] does not coincide with the original one proposed for DPH because in [18] Arrizón includes certain binary factors which are intended to separate noise from the signal in the reconstruction plane. More recently, simultaneous and independent amplitude and phase modulation that utilizes the DPH representation was proposed [19]. In the above work, two adjacent pixels of a phase SLM are superimposed for interference by using polarization-sensitive components.

On the other hand, $4-f$ optical systems allow for the implementation of different phase coding techniques by using SLMs as well as different types of spatial filters in the Fourier plane. For instance, a $4-f$ optical system with a phase grating filter placed in the Fourier plane was employed to combine two phase holograms in DPH configuration that are displayed in symmetrically separate regions of a SLM [20]. In addition, the encoding of arbitrary scalar complex fields with three types of computer-generated holograms reconstructed by spatial filtering in the Fourier spectrum plane was discussed in [4]. Recently, effects of the shape of the Fourier filters on the quality of the reconstructed complex field obtained at the output a $4-f$ optical system were investigated [7]. In [7], each pixel at the output plane was encoded by an array of $N \times N$ subpixels of the phase hologram. This also happens with the codification employed in [8], where a method for performing binary intensity and continuous phase modulation of beams with a SLM and a low-pass spatial filtering $4-f$ system is introduced.

In this Letter, we propose a single-pixel on-axis technique based on DPH to approximately encode a complex field $U(x, y)$ into a phase-only optical element. The reconstruction of $U(x, y)$ is achieved at the output plane of a $4-f$ optical system, after applying a low-pass filter in the Fourier plane. We theoretically demonstrate that for band-limited functions, that is, functions with Fourier

transforms that are nonzero over only a finite region of the frequency space, the proposed encoding technique allows for an exact retrieval of the spectrum of $U(x,y)$ just after the filter.

To obtain the encoding function, we represent the functions $e^{i\theta(x,y)}$ and $e^{i\vartheta(x,y)}$ (for $A_{\max} \equiv 2$, and then $B = 1$) by arrays of their sampled values $M_1(x,y)e^{i\theta(x,y)}$ and $M_2(x,y)e^{i\vartheta(x,y)}$ at a given input plane. The functions $M_1(x,y)$ and $M_2(x,y)$ hold for the transmittance of complementary two-dimensional binary gratings (checkerboard patterns) taken at the Nyquist limit, such as $M_1(x,y) + M_2(x,y) = 1$. It can be shown these checkerboard patterns can be described by the following expressions:

$$M_{1,2}(x,y) = \frac{1}{2}\sum_{n=-\infty}^{\infty}\sum_{m=-\infty}^{\infty}\Lambda_{1,2}(n,m)e^{i\frac{2\pi n x}{p}}e^{i\frac{2\pi m y}{p}}, \quad (1)$$

$$\Lambda_{1,2}(n,m) \equiv \cos\left[\frac{\pi(n \pm m)}{2}\right]\text{sinc}\left(\frac{n}{2}\right)\text{sinc}\left(\frac{m}{2}\right). \quad (2)$$

In Eqs. (1) and (2), $\text{sinc}(\xi) \equiv \sin(\pi\xi)/(\pi\xi)$ represents the sinc function of argument ξ, p is the period of the two-dimensional binary gratings, and the numbers n, m will denote their diffraction orders. The difference between $M_1(x,y)$ and $M_2(x,y)$ is only given by the sign of the sum within the argument of the cosine in Eq. (2). In Fig. 1, the functions $M_1(x,y)$ and $M_2(x,y)$ are evaluated within the intervals $x = y = [-p,p]$ up to 300 steps of the sums for the variables n, m with $p = 16\ \mu\text{m}$.

As far as the above steps are incremented, the functions $M_1(x,y)$ and $M_2(x,y)$ approach better the checkerboard patterns. In addition, owing to the fact that the sampled values are located at different spatial positions in the input plane, the following equality takes place:

$$M_1(x,y)e^{i\theta(x,y)} + M_2(x,y)e^{i\vartheta(x,y)} = e^{i\alpha(x,y)}, \quad (3)$$

$$\alpha(x,y) = M_1(x,y)\theta(x,y) + M_2(x,y)\vartheta(x,y). \quad (4)$$

In Eqs. (3) and (4), the phase term $\alpha(x,y)$ will be the desired encoding function. Here, it should be noted that, at the input plane, the complex field $U(x,y)$ cannot be approximated by the function $e^{i\alpha(x,y)}$, because at this plane the functions $e^{i\theta(x,y)}$ and $e^{i\vartheta(x,y)}$ do not interfere at all. At this point, we assume that $U(x,y)$ is a band-limited function, and determine the spectrum $H(u,v)$ of the function $e^{i\alpha(x,y)}$ by using the following Fourier transform definition:
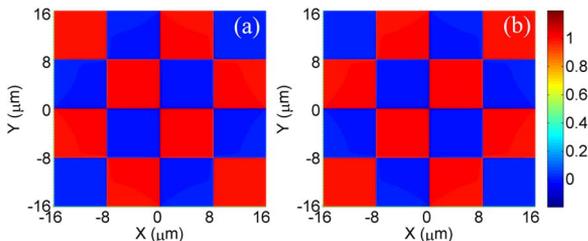

Fig. 1. Checkerboard patterns obtained with functions (a) $M_1(x,y)$ and (b) $M_2(x,y)$, respectively.

$$H(u,v) = F\{e^{i\alpha(x,y)}\} \equiv \int_{-\infty}^{\infty}\int_{-\infty}^{\infty} e^{i\alpha(x,y)}e^{-i\frac{2\pi(x'x+y'y)}{f\lambda}}\,\text{d}x\text{d}y. \quad (5)$$

In Eq. (5), the distance between the input plane and the Fourier plane is denoted by f, λ represents the wavelength of light, and the coordinates u and v in the frequency space are given by $u = x'/f\lambda$ and $v = y'/f\lambda$. From Eqs. (3) and (4), after applying the convolution theorem, the spectrum $H(u,v)$ can be expressed as

$$H(u,v) = \frac{1}{2}[H_1(u,v) + H_2(u,v)], \quad (6)$$

$$H_1(u,v) = \sum_{n=-\infty}^{\infty}\sum_{m=-\infty}^{\infty}\Lambda_1(n,m)\Psi\left(u - \frac{n}{p}, v - \frac{m}{p}\right), \quad (7)$$

$$H_2(u,v) = \sum_{n=-\infty}^{\infty}\sum_{m=-\infty}^{\infty}\Lambda_2(n,m)\Omega\left(u - \frac{n}{p}, v - \frac{m}{p}\right). \quad (8)$$

In Eqs. (7) and (8), $\Psi(u,v) = F\{e^{i\theta(x,y)}\}$ and $\Omega(u,v) = F\{e^{i\vartheta(x,y)}\}$. The band-limited condition ensures that the spectrum $H(u,v)$ is nonzero over only a finite region of the frequency space. Now, from Eqs. (6)–(8) it follows that this region is about the points $(n/p, m/p)$, that correspond to the diffraction orders of the phase optical element $\alpha(x,y)$. Furthermore, if the period p of the gratings $M_1(x,y)$ and $M_2(x,y)$ is sufficiently small, the spatial frequency separations $1/p$ among diffraction orders will be great enough to guarantee that adjacent diffraction orders do not overlap. At the Nyquist limit of the above gratings the maximum spatial frequency separation is theoretically achieved. From Eqs. (6)–(8) it is easy to see that if we use a filter $P(u,v)$ to block all diffraction orders but the zero one, the spectrum is reduced to the expression

$$H(u,v)P(u,v) = \frac{1}{2}F\{U(x,y)\}, \quad (9)$$

where

$$F\{U(x,y)\} \equiv \Psi(u,v) + \Omega(u,v). \quad (10)$$

This is the main theoretical result of our manuscript. On one hand, Eqs. (9) and (10) show that by using the single pixel encoding function given in Eq. (4) we are able to exactly retrieve the full spectrum $F\{U(x,y)\}$ of the original complex field $U(x,y)$ in the Fourier plane, about the zero diffraction order. In addition, at the output plane, after Fourier transform of the filtered Fourier plane we find, without including irrelevant constant factors, the convolution of the magnified spatially reversed complex field with the Fourier transform of the filter, that is, $U(-x/Mag, -y/Mag) \otimes F\{P(u,v)\}$. The output plane is located now at the distance g from the Fourier plane, and the corresponding magnification factor is $Mag = g/f$.

Owing to the characteristics of the filter $P(u,v)$, the previous convolution operation gives us an approximate

description of the complex field. To clarify this aspect, we consider a particular case of a filter in the frequency domain given by the two-dimensional rectangle function $P(u, v) = \text{rect}[u/(\varepsilon/f\lambda), v/(\varepsilon/f\lambda)]$, where $\varepsilon = f\lambda/p$. The value of ε was taken from Eq. (6) as the distance from the propagation axis to the first diffraction order. Note that, the above filter meets with Eq. (9), and its Fourier transform yields

$$F\{\text{rect}(x'/\varepsilon, y'/\varepsilon)\} \propto \frac{\sin\left(\frac{\pi}{pMag}x\right)}{\pi x} \frac{\sin\left(\frac{\pi}{pMag}y\right)}{\pi y}. \quad (11)$$

As far as the parameter $\pi/pMag$ tens to infinity, the function described by Eq. (11) approaches to the two-dimensional Dirac delta function $\delta_{\text{Dirac}}(x, y)$. In this case $U(-x/Mag, -y/Mag) \otimes \delta_{\text{Dirac}}(x, y) \equiv U(-x/Mag, -y/Mag)$ and the complex field at the output plane is completely retrieved. In practice, as the convolution operation cannot be avoided, the spatial resolution of the reconstructed amplitude and phase at the output plane is lower than that of the original $A(x, y)$ and $\varphi(x, y)$ functions.

In order to experimentally corroborate the encoding technique discussed above, we implement the optical setup given in Fig. 2. The quasi-monochromatic laser beam emitted from a Ti: sapphire laser oscillator (Femtosource, Femtolaser), working without mode-locking, is used as a light source. In this condition, the laser beam has a narrow spectral line centered at wavelength $\lambda = 800$ nm. Before it impinges onto a reflective liquid crystal on silicon phase-only SLM (Holoeye Pluto), the beam is conveniently attenuated with neutral filters (NF), and spatially magnified by using a commercial beam expander (BE). The desired phase element $\alpha(x, y)$ is encoded into the SLM that has 1920×1080 pixels and 8 µm of pixel pitch. The first beam splitter (BS$_1$) allows for both the normal incident onto the SLM, and its backreflection forward a $4-f$ imaging system. The input plane of this optical system coincides with the SLM plane. The $4-f$ imaging system is made up of a couple of identical refractive lenses (L) with focal length of 150 mm. At the Fourier plane, the beam is transmitted through a low-pass spatial filter that consists of an iris of radius $\varepsilon/2$. The second beam splitter (BS$_2$) is used to simultaneously align both a CMOS camera (Ueye UI-1540M, 1280×1024 pixel resolution and 5.2 pixel pitch), and a Shack–Hartmann wavefront sensor (SH-WS) at the output of the $4-f$ optical system. The CMOS camera (CAM) records the amplitude of
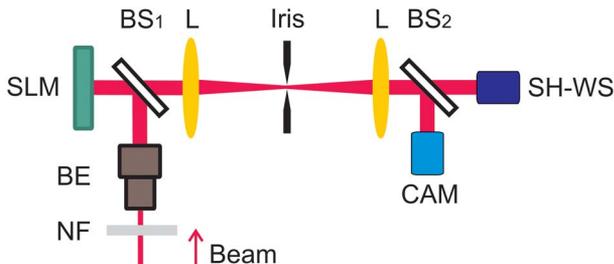
the reconstructed complex field, and the SH-WS is intended to measure its phase.

In Fig. 3, the initial and retrieved amplitude and phase functions within a square spatial window of [3 mm × 3 mm] are shown. For this experiment we use two complex field functions whose amplitudes are composed of the well-known Lena and Cameraman images, whereas their phases are $\varphi(x, y) = \pi/2 \sin[2\pi x/(5\lambda)]\cos[2\pi y/(5\lambda)]$ and $\varphi(x, y) = \pi/2 \sin[500\pi(x^3 + y^3)/\lambda]$, respectively. The mean square error between the normalized data from theory and experiment yields 1.7% for Figs. 3(a) and 3(b), 2.8% for Figs. 3(c) and 3(d), 6.4% for Figs. 3(e) and 3(f), and 5.2% for Figs. 3(g) and 3(h). We believe that small differences among them come mainly from two causes. The first one is the decreasing of the spatial resolution of the recovered amplitude and phase data due to the above-mentioned convolution operation. This convolution is affected by the value of ε, which is inversely proportional to the pixel size of the SLM. The second reason is the low spatial resolution of the SH-WS, which is unable to resolve phase functions with spatial structure below its lenslet pitch (150 µm for our SH-WS).

The phase encoding conditions imposed by the modulation range of our SLM (almost 3π for normal incident), as well as the limited phase range $[-\pi/2, \pi/2]$ used to encode the amplitude if $A_{\min} = 0$ can also affect the quality of the measured data. The term $A_{\min}$ holds for the

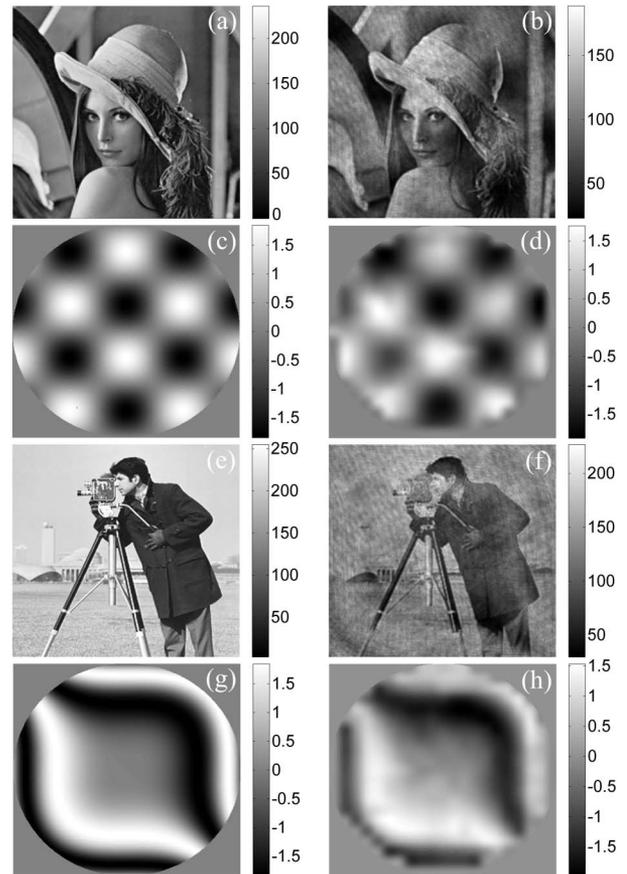Fig. 2. Schematic setup used to measure the amplitude and phase of a complex field.

Fig. 3. Experimental results. (a), (e) Initial amplitude and (c), (g) phase of the complex field, and corresponding (b), (f) amplitude and (d), (h) phase measured. All data are shown within a square window of [3 mm × 3 mm].

minimum value of $A(x, y)$. We find out that the contrast of the image recorded by the camera depends on percent of modulation range employed to encode $A(x, y)$.

In this experiment, the phase range dedicated to encode the amplitude was increased up to the range $[-\pi, \pi]$ by setting $A_{min} = -1$. This allows us to improve the contrast of the measured amplitude image at expense of decreasing the phase range used to encode $\varphi(x, y)$.

The sampling technique described by Eq. (3) is similar to the random mask encoding technique of multiplexing phase-only filters [21], later adapted to the generation of holographic optical tweezers [22]. The main difference between both techniques is given by the selection of the complementary binary functions. In this manuscript these functions are determined by two complementary checkerboard patterns taken at the Nyquist limit, whereas in [21] and [22] they are generated following a random procedure. Recently, a stack of random resampling masks are also used to propose a robust method for rapidly reducing the incoherent noise in digital holography [23]. Furthermore, the encoding method presented in [22] consists of the Fourier transform of N linear phase functions, sampled previously into a SLM by spatially disjoint binary masks. In contrast, by using the encoding method discussed here one can directly reconstruct the complex field obtained from the linear superposition of phase functions. Here it should be emphasized additional features of our method. The encoding function given in Eq. (4) allows for a single-pixel mathematical operation, instead of using an iterative algorithm and/or an array of $N \times N$ subpixels to codify each pixel of the input plane. This allows for quite dynamic and extremely fast computation process. The information of the complex field is recovered with an accuracy that strongly depends on the minimum feature size of the encoded phase element. The smaller the pixel size, the better.

References

1. J. P. Kirk and A. L. Jones, J. Opt. Soc. Am. **61**, 1023 (1971).
2. J. A. Davis, D. M. Cottrell, J. Campos, M. J. Yzuel, and I. Moreno, Appl. Opt. **38**, 5004 (1999).
3. P. Birch, R. Young, D. Budgett, and C. Chatwin, Opt. Lett. **26**, 920 (2001).
4. V. Arrizón, Opt. Lett. **28**, 2521 (2003).
5. E. Bolduc, N. Bent, E. Santamato, E. Karimi, and R. W. Boyd, Opt. Lett. **38**, 3546 (2013).
6. R. W. Cohn and M. Liang, Appl. Opt. **33**, 4406 (1994).
7. T. Sarkadi, Á. Kettinger, and P. Koppa, Appl. Opt. **52**, 5449 (2013).
8. Z. Göröcs, G. Erdei, T. Sarkadi, F. Ujhelyi, J. Reményi, P. Koppa, and E. Lórincz, Opt. Lett. **32**, 2336 (2007).
9. J.-P. Liu, W.-Y. Hsieh, T.-C. Poon, and P. Tsang, Appl. Opt. **50**, H128 (2011).
10. J. L. Horner and J. R. Leger, Appl. Opt. **24**, 609 (1985).
11. J. Campos, A. Márquez, M. J. Yzuel, J. A. Davis, D. M. Cottrell, and I. Moreno, Appl. Opt. **39**, 5965 (2000).
12. A. A. S. Awwal, M. A. Karim, and S. R. Jahan, Appl. Opt. **29**, 233 (1990).
13. P. C. Mogensen and J. Glückstad, Opt. Lett. **25**, 566 (2000).
14. A. M. Weiner, S. Oudin, D. E. Leaird, and D. H. Reitze, J. Opt. Soc. Am. A **10**, 1112 (1993).
15. A. Dudley, R. Vasilyeu, V. Belyi, N. Khilo, P. Ropot, and A. Forbes, Opt. Commun. **285**, 5 (2012).
16. C. K. Hsueh and A. A. Sawchuk, Appl. Opt. **17**, 3874 (1978).
17. V. Arrizón, Opt. Lett. **28**, 1359 (2003).
18. V. Arrizón, U. Ruiz, R. Carrada, and L. A. González, J. Opt. Soc. Am. A **24**, 3500 (2007).
19. S. Reichelt, R. Häussler, G. Fütterer, N. Leister, H. Kato, N. Usukura, and Y. Kanbayashi, Opt. Lett. **37**, 1955 (2012).
20. H. Song, G. Sung, S. Choi, K. Won, H.-S. Lee, and H. Kim, Opt. Express **20**, 29844 (2012).
21. J. A. Davis and D. M. Cottrell, Opt. Lett. **19**, 496 (1994).
22. M. Montes-Usategui, E. Pleguezuelos, J. Andilla, and E. Martín-Badosa, Opt. Express **14**, 2101 (2006).
23. V. Bianco, M. Paturzo, P. Memmolo, A. Finizio, P. Ferraro, and B. Javidi, Opt. Lett. **38**, 619 (2013).